Numerical computation of Stephenson's g-functions in multiply connected domains

Christopher C. Green[a] & Mohamed M S Nasser[a]

[a]Department of Mathematics, Statistics & Physics, Wichita State University, Wichita, KS 67260-0033, USA

`christopher.green@wichita.edu, mms.nasser@wichita.edu`

Abstract

There has been much recent attention on h-functions, so named since they describe the distribution of harmonic measure for a given multiply connected domain with respect to some basepoint. In this paper, we focus on a closely related function to the h-function, known as the g-function, which originally stemmed from questions posed by Stephenson in [3]. Computing the values of the g-function for a given planar domain and some basepoint in this domain requires solving a Dirichlet boundary value problem whose domain and boundary condition change depending on the input argument of the g-function. We use a well-established boundary integral equation method to solve the relevant Dirichlet boundary value problems and plot various graphs of the g-functions for different multiply connected circular and rectilinear slit domains.

Keywords. g-function, multiply connected domain, conformal mapping, boundary integral equation, generalized Neumann kernel

1 Introduction

Let Ω be a domain in the extended complex plane $\overline{\mathbb{C}} = \mathbb{C} \cup \{\infty\}$ and let z_0 be a given basepoint in Ω. We assume that Ω is either an unbounded domain of connectivity ℓ or a bounded domain of connectivity $\ell+1$ where $\ell \geq 1$ (for example, see Figures 1 and 2 when $\ell = 4$). For $r > 0$, let Ω_r be the connected component of $\Omega \cap B(z_0, r)$ which contains z_0 and let $E_r = \partial \Omega_r \cap \overline{B(z_0, r)}$ where $B(z_0, r)$ is the open disk with center z_0 and radius r. Unlike the given domain Ω, the domain Ω_r is not fixed and changes as r increases. Note that the domain Ω_r is always bounded with $m+1$ boundary components, where $0 \leq m \leq \ell$ (i.e., the domain Ω_r could be simply connected or multiply connected depending on r). We refer to $\partial B(z_0, r)$ as a 'capture circle' of radius r and center z_0 and we denote it by $\mathcal{C}_r$.

For $E_r \neq \emptyset$ and $\partial \Omega_r \backslash E_r \neq \emptyset$, the harmonic measure of E_r with respect to Ω_r is the $C^2(\Omega_r)$ function $u : \Omega_r \to (0, 1)$ satisfying the Laplace equation

$$\nabla^2 u = 0$$

in Ω_r, with $u(z) \to 1$ when $z \to E_r$ and $u(z) \to 0$ when $z \to \partial \Omega_r \backslash E_r$. Harmonic measure is a key concept in potential theory and has numerous applications to geometric function theory [1, 4, 6, 11, 27]. The harmonic measure of E_r with respect to Ω_r calculated at the point $z \in \Omega_r$ will be denoted by $\omega_{\mathrm{hm}}(z, E_r, \Omega_r)$.

The Stephenson's g-function (henceforth referred to simply as the 'g-function') associated with the domain Ω with respect to the basepoint z_0, $g : [0, \infty) \mapsto [0, 1]$, is defined by

$$g(r) = \omega_{\mathrm{hm}}(z_0, E_r, \Omega_r) \tag{1}$$

where $g(0) = 0$. The g-function, which was first introduced in [3, Problem 6.116], is a non-decreasing piecewise continuous function. It follows from this definition of the g-function
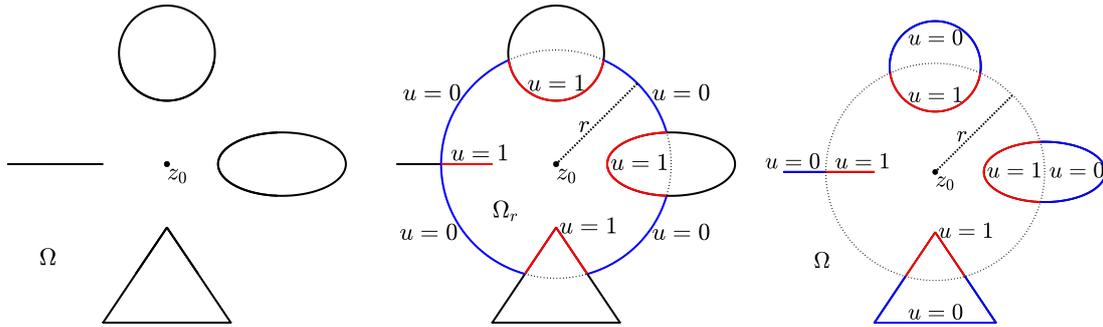
Figure 1: Schematics of an example of an unbounded domain Ω and a basepoint $z_0 \in \Omega$ (left), the domain Ω_r with the boundary conditions and the capture circle $\mathcal{C}_r$ for the g-function (center), and the domain Ω with the boundary conditions and the capture circle for the h-function (right).
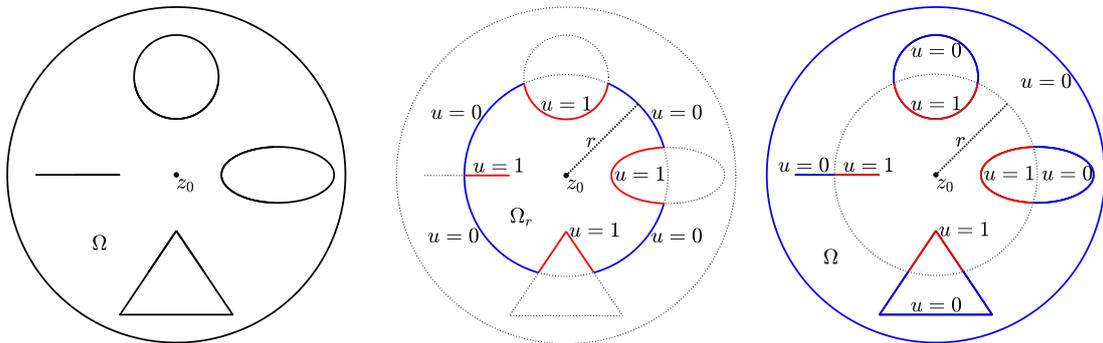
Figure 2: Schematics of an example of a bounded domain Ω and a basepoint $z_0 \in \Omega$ (left), the domain Ω_r with the boundary conditions and the capture circle $\mathcal{C}_r$ for the g-function (center), and the domain Ω with the boundary conditions and the capture circle for the h-function (right).

that $g(r) = u(z_0)$ where $u(z)$ is the unique solution of the following Dirichlet boundary value problem (BVP):

$$\nabla^2 u(z) = 0, \qquad z \in \Omega_r; \tag{2a}$$
$$u(z) = \gamma(z), \qquad z \in \partial\Omega_r; \tag{2b}$$

where

$$\gamma(z) = \begin{cases} 1, & z \in E_r, \\ 0, & z \in \partial\Omega_r \backslash E_r. \end{cases} \tag{3}$$

This is illustrated in Figure 1 for unbounded multiply connected domains Ω and in Figure 2 for bounded domains. See also Figures 3 and 4 when the domain Ω is the doubly connected domain exterior to two circles (Figure 3) and exterior to two slits (Figure 4) with the basepoint fixed to be at $z_0 = 0$.

The function which is strongly associated with the g-function is the so-called harmonic-measure distribution function, dubbed the h-function, which is defined also with respect to the planar domain Ω and the basepoint z_0. It is equal to the value of the harmonic measure of the portion E_r of the boundary with respect to Ω at z_0:

$$h(r) = \omega_{\mathrm{hm}}(z_0, E_r, \Omega).$$

The h-function can be computed by solving a Dirichlet boundary value problem similar to (2). This is illustrated also in Figure 1 for unbounded multiply connected domains Ω and in Figure 2 for bounded domains.
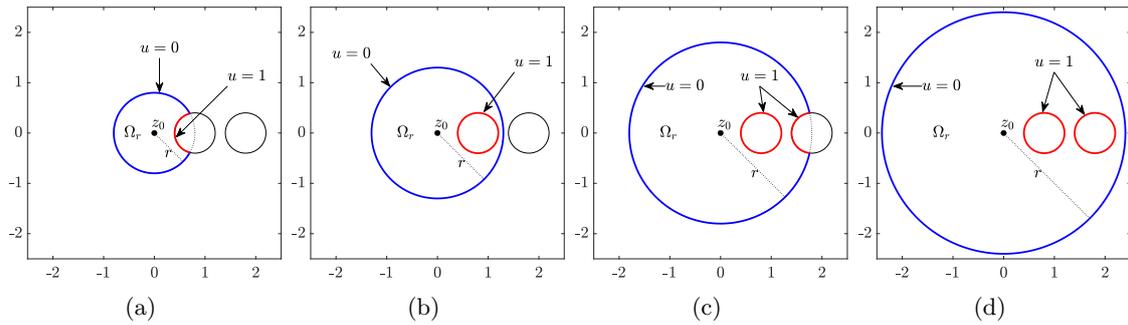
Figure 3: Schematics of the four different domain regimes Ω_r as the radius r of the capture circle $\mathcal{C}_r$ increases for the doubly connected domain Ω exterior to two disks of equal radius 0.4 centered at 0.8 and 1.6 with the basepoint $z_0 = 0$. Here, $m = 0$ in (a), $m = 1$ in (b) and (c), and $m = 2$ in (d).
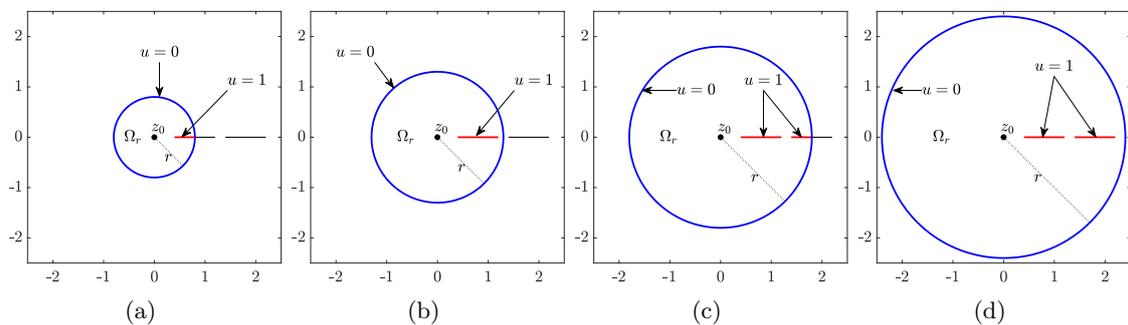
Figure 4: Schematics of the four different domain regimes Ω_r as the radius r of the capture circle $\mathcal{C}_r$ increases for the doubly connected domain Ω exterior to the two segments $[0.4, 1.2]$ and $[1.4, 2.2]$ of equal length with the basepoint $z_0 = 0$. Here, $m = 0$ in (a), $m = 1$ in (b) and (c), and $m = 2$ in (d).

Naturally, owing to the connection with harmonic measure, a physical interpretation of the values of the g-functions – as for the h-functions – can be given in terms of a Brownian particle released into Ω from the point z_0 (see [12, 13, 14, 26] for the relation between Brownian motion and harmonic functions). More precisely, for each assignment of r, the value $g(r)$ is the probability that the Brownian particle will first exit the domain Ω_r through the portion E_r of the boundary $\partial\Omega_r$. These hitting probabilities described by the g-function have particle trajectories which are confined strictly to the interior of the capture circle. On the other hand, given an $r > 0$, the value $h(r)$ is the probability that a Brownian walker will first exit the domain Ω through the portion E_r of the boundary $\partial\Omega$. In terms of the set of admissible trajectories of the Brownian particle, there may be trajectories which wander into the exterior of the capture circle. By the monotonicity of harmonic measure [11, p. 252], it can be shown that $g(r) \leq h(r)$ for a given domain Ω and a given basepoint z_0. Further, if Ω is unbounded, then the value of the h-function will be 1 when the capture circle covers all the boundary components of Ω. However, the g-function will never attain the value 1 when Ω is unbounded even if all boundary components have been covered by the capture circle: $g(r) \to 1$ as $r \to \infty$. On the other hand, for a bounded domain Ω, the value of both functions will be 1 when the capture circle covers all the boundary components of Ω. A schematic illustrating the main differences between the g-function and the h-function is given in Figure 1 when Ω is an unbounded domain and in Figure 2 when Ω is a bounded domain.

The computation of the h-function has been the subject of several recent works. In [9, 7], analytic formulas have been derived using the Schottky–Klein prime function

for computing the h-function associated with several multiply connected circular and slit domains. In [8], a boundary integral equation methods has been presented for the computation of the h-function of a class of highly multiply connected symmetrical slit domains. For more information about the h-function and its computation, we refer the reader to [2, 7, 8, 9, 15, 16, 17, 18, 26, 28].

Despite this body of work on the h-functions, the study of g-functions has so far received much less attention. Analytic formulas for the g-function for several simply connected domains has been presented recently in [16, 19]. In this paper, we present a boundary integral equation method for the numerical computation of the g-function in multiply connected domains. The proposed method is used effectively in this paper to make calculations of the g-functions associated with multiply connected circular and rectilinear slit domains. To the best of our knowledge, this is the first attempt to compute the g-function for multiply connected domains.

The layout of this paper is as follows. In Section 2, we describe a boundary integral equation method that will be used to compute the g-function in this paper. In Sections 3 and 4, we compute the g-function for unbounded multiply connected circular and rectilinear slit domains, respectively. In Section 5, we discuss the computation of the g-functions for other kinds of circular domains. Examples of g-functions in bounded domains are presented in Section 6. Finally, we make concluding remarks in Section 7.

2   The integral equation method

Let G be a bounded simply or multiply connected domain whose boundary components are piecewise smooth Jordan curves. In this section, we outline a boundary integral equation (BIE) method for solving the following BVP:

$$\nabla^2 u(z) = 0, \qquad z \in G; \tag{4a}$$

$$u(z) = \gamma(z), \qquad z \in \Gamma = \partial G; \tag{4b}$$

in the domain G where γ is assumed to be a Hölder continuous function on the boundary Γ. The domain G is related to the domain Ω_r introduced in the previous section. When the boundary components of Ω_r are piecewise smooth Jordan curves, we assume that $G = \Omega_r$ (see Section 3). If some of the boundary components of Ω_r are slits, then we will compute numerically a conformally equivalent domain G whose boundaries are piecewise smooth Jordan curves (see Section 4). That is, G is always assumed to be a bounded multiply connected domain of connectivity $m+1$ with piecewise smooth boundaries where $0 \leq m \leq \ell$ (note that G is simply connected when $m = 0$). The method presented in this section will be used later to solve the BVP (2) for various g-functions.

Let
$$\Gamma = \partial G = \Gamma_0 \cup \Gamma_1 \cup \cdots \cup \Gamma_m$$

where Γ_0 is the external boundary and oriented counterclockwise. The inner curves $\Gamma_1, \ldots, \Gamma_m$ are oriented clockwise. Each curve Γ_k is parametrized by $\eta_k(t)$ for $t \in J_k = [0, 2\pi]$, $k = 0, 1, \ldots, m$. If Γ_k has corner points (but not cusps), we parametrize it as explained in [24]. Let J be the disjoint union of the $m + 1$ intervals $J_j = [0, 2\pi]$, $j = 0, 1, \ldots, m$. We define a parametrization of the whole boundary Γ on J by

$$\eta(t) = \begin{cases} \eta_0(t), & t \in J_0, \\ \eta_1(t), & t \in J_1, \\ \quad \vdots \\ \eta_m(t), & t \in J_m. \end{cases}$$

With the parametrization $\eta(t)$, we define a complex function A by

$$A(t) = \eta(t) - \alpha, \quad t \in J, \tag{5}$$

where α is a given point in the domain G. The generalized Neumann kernel $N(s,t)$ is defined for $(s,t) \in J \times J$ by

$$N(s,t) = \frac{1}{\pi} \, \mathrm{Im} \left(\frac{A(s)}{A(t)} \frac{\eta'(t)}{\eta(t) - \eta(s)} \right). \tag{6}$$

We define also the following kernel

$$M(s,t) = \frac{1}{\pi} \, \mathrm{Re} \left(\frac{A(s)}{A(t)} \frac{\eta'(t)}{\eta(t) - \eta(s)} \right), \tag{7}$$

for $(s,t) \in J \times J$. The integral operators with the kernels $N(s,t)$ and $M(s,t)$ are denoted by $\mathbf{N}$ and $\mathbf{M}$, respectively. Further details can be found in [21, 22, 29].

For a given continuous function γ, the Dirichlet problem (2) has a unique solution $u(z)$ in G. This unique solution can be regarded as the real part of an analytic function $F(z)$ in G which is not necessarily single-valued for $m > 0$. However, the function $F(z)$ can be written as

$$F(z) = c + (z - \alpha)f(z) - \sum_{j=1}^{m} a_j \log(z - \alpha_j) \tag{8}$$

where each α_j is a given point in the domain interior to the boundary component Γ_j, $j = 1, 2, \ldots, m$, and $a_1, \ldots, a_m$ are undetermined real constants [20]. Since we are interested in the real part of $F(z)$, we assume that c is real which is also undetermined. It then follows that $f(z)$ satisfies the Riemann–Hilbert problem [25, 29]

$$\mathrm{Re}[A(t)f(\eta(t))] = -c + \gamma_0(t) + \sum_{j=1}^{m} a_j \gamma_j(t) \tag{9}$$

where $\gamma_0(t) = \gamma(t)$ and

$$\gamma_j(t) = \log|\eta(t) - \alpha_j|, \quad t \in J, \quad j = 1, 2, \ldots, m. \tag{10}$$

Note that solving the Riemann–Hilbert problem (9) requires finding the unknown analytic function $f(z)$ as well as the $m+1$ unknown real constants $c, a_1, \ldots, a_m$ on the right-hand side of (9).

We choose $\alpha = z_0$, the basepoint, and hence

$$u(z_0) = \mathrm{Re}[F(z_0)] = c - \sum_{j=1}^{m} a_j \log|z_0 - \alpha_j|. \tag{11}$$

Thus computing $u(z_0)$ requires finding only the $m+1$ real constants $c, a_1, \ldots, a_m$. These constants will be computed using a method based on a boundary integral equation with the generalized Neumann kernel described below.

For each j, $j = 0, 1, \ldots, m$, there exists a unique real function $\mu_j(t)$ and a unique piecewise constant function $\nu_j(t)$ [25, Theorem 2]:

$$\nu_j(t) = \nu_{k,j}, \quad t \in J_k, \quad k = 0, 1, \ldots, m,$$

with real constants $\nu_{0,j}, \nu_{1,j}, \ldots, \nu_{m,j}$, such that

$$f_j(\eta(t)) = (\gamma_j(t) + \nu_j(t) + \mathrm{i}\mu_j(t))/A(t) \tag{12}$$

are the boundary values of an analytic function $f_j(z)$ in the bounded domain G. The function μ_j is the unique solution of the boundary integral equation

$$(\mathbf{I} - \mathbf{N})\mu_j = -\mathbf{M}\gamma_j; \tag{13}$$

and the function ν_j is given by

$$\nu_j = [\mathbf{M}\mu_j - (\mathbf{I} - \mathbf{N})\gamma_j]/2. \tag{14}$$

With the analytic functions $f(z)$ in (9) and $f_0(z), f_1(z), \ldots, f_m(z)$ in (12), we define an analytic function $F(z)$ in G by

$$\tilde{f}(z) = f_0(z) + \sum_{j=1}^{m} a_j f_j(z) - f(z).$$

The function $\tilde{f}(z)$ satisfies the Riemann–Hilbert problem

$$\mathrm{Re}[A(t)\tilde{f}(\eta(t))] = \nu_0(t) + \sum_{j=1}^{m} a_j \nu_j(t) + c$$

where the right-hand side is a piecewise constant function. It then follows from [25, Lemma 2] that

$$\nu_0(t) + \sum_{j=1}^{m} a_j \nu_j(t) + c = 0.$$

Hence, the $m + 1$ unknown real constants $c, a_1, \ldots, a_m$ are the components of the unique solution vector of the linear system

$$\begin{bmatrix} \nu_{0,1} & \cdots & \nu_{0,m} & 1 \\ \nu_{1,1} & \cdots & \nu_{1,m} & 1 \\ \vdots & \ddots & \vdots & \\ \nu_{m,1} & \cdots & \nu_{m,m} & 1 \end{bmatrix} \begin{bmatrix} a_1 \\ \vdots \\ a_m \\ c \end{bmatrix} = \begin{bmatrix} -\nu_{0,0} \\ -\nu_{1,0} \\ \vdots \\ -\nu_{m,0} \end{bmatrix}. \tag{15}$$

The matrix of this linear system is a particular case of the matrix in the linear system in [25, Theorem 4] and the proof of the uniqueness of the solution of the linear system then follows.

When the capture circle does not intersect any of the boundary components (as in Figures 3(b,d)), then the function γ assumes the following simple form:

$$\gamma(t) = \begin{cases} 0, & t \in J_0, \\ 1, & t \in J_1, \\ \vdots & \\ 1, & t \in J_m. \end{cases} \tag{16}$$

Hence, the function $f_0(z)$ satisfies the Riemann–Hilbert problem

$$\mathrm{Re}[A(t)f_0(\eta(t))] = \gamma_0(t) + \nu_0(t) \tag{17}$$

where $\gamma_0(t) = \gamma(t)$. Here, the right-hand side is a piecewise constant function which implies that $\gamma_0(t) + \nu_0(t) = 0$ and hence the right-hand side of the linear system (15) will be the vector $[0, 1, \ldots, 1]^T$.

It is clear from (13) and (14) that computing the $m + 1$ real constants $c, a_1, \ldots, a_m$ requires solving the same integral equation with the generalized Neumann kernel (13) but with $m + 1$ different right-hand sides and to compute the function ν in (14) $m + 1$ times. When the capture circle does not intersect any of the boundary components, these numbers both reduce to m.

In this paper, we use the MATLAB function `fbie` from [22] to approximate the solution of the integral equation (13) and the function ν in (14). In the function `fbie`, the integral equation (13) is discretized by the Nyström method and the trapezoidal rule. This leads

to an $(m+1)n \times (m+1)n$ linear system with a dense non-symmetric coefficient matrix, where n is the number of nodes in the discretization of each boundary component. This linear system is then solved by the MATLAB's built-in `gmres` function together with the MATLAB function `zfmm2dpart` from the Fast Multipole Method (FMM) toolbox FMMLIB2D [10]. This method has been used in several publications including domains with high connectivity, domains with corners, and slits domains. We will not present further details here and instead refer the readers to [8, 23, 24, 25]. However, all MATLAB codes for the calculations presented in this paper are available at: `https://github.com/mmsnasser/gf`.

3 Domains bounded by circles

Let Ω be an unbounded multiply connected domain in the exterior of ℓ non-overlapping circles $C_1, C_2, \ldots, C_\ell$ with centers $z_1, \ldots, z_\ell$ and radii $r_1, \ldots, r_\ell$, and let $z_0 \in \Omega$ be a given basepoint. We define
$$\delta_k = |z_0 - z_k|, \quad k = 1, 2, \ldots, \ell.$$

We assume that these circles are arranged such that $\delta_1 < \delta_2 < \cdots < \delta_\ell$. Further, for a given $r > 0$, we assume that the capture circle $\mathcal{C}_r$ intersects with at most one of the circles $C_1, C_2, \ldots, C_\ell$ (see Figure 3 for an example when $\ell = 2$).

There are two classes of boundary data to be considered as in the following two subsections.

3.1 Continuous boundary data

Suppose that the capture circle $\mathcal{C}_r$ does not intersect any of the circles $C_1, \ldots, C_\ell$. For $m = 0, 1, 2, \ldots, \ell$, we assume that the circles $C_1, \ldots, C_m$ are inside $\mathcal{C}_r$ and the circles $C_{m+1}, \ldots, C_\ell$ are outside $\mathcal{C}_r$. That is, all circles $C_1, \ldots, C_m$ are outside the capture circle $\mathcal{C}_r$ for $m = 0$ and all circles $C_1, \ldots, C_\ell$ are inside the capture circle $\mathcal{C}_r$ for $m = \ell$. See Figure 3(b,d) for $m = 1$ and 2, respectively.

Note that $g(r) = 0$ for all values of r such that all the circles $C_1, \ldots, C_\ell$ are outside the capture circle $\mathcal{C}_r$ (i.e. $m = 0$). Otherwise, if $m > 0$, then the circles $C_1, \ldots, C_m$ are inside $\mathcal{C}_r$ and the circles $C_{m+1}, \ldots, C_\ell$ are outside $\mathcal{C}_r$. In this case, the domain Ω_r is a bounded multiply connected domain of connectivity $m + 1$ and

$$\partial\Omega_r = C_1 \cup \cdots \cup C_m \cup \mathcal{C}_r.$$

Here, the domain Ω_r is of the type of domain G considered in Section 2 with $\Gamma_0 = \mathcal{C}_r$ and $\Gamma_k = C_k$ for $k = 1, \ldots, m$. Note that, in the BVP (2), we have $E_r = C_1 \cup \cdots \cup C_m$ and hence $\partial\Omega_r \backslash E_r = \mathcal{C}_r$. Thus, $u(z)$ is the unique solution of the Dirichlet problem (4) with the function $\gamma(t)$ as in (16), i.e., the function $u(z)$ is the harmonic measure of $C_1 \cup \cdots \cup C_m$ with respect to the domain Ω_r. It then follows from (1) and (11) that

$$g(r) = u(z_0) = c - \sum_{j=1}^{m} a_j \log |z_0 - \alpha_j|$$

where the $m + 1$ unknown real constants $c, a_1, \ldots, a_m$ are obtained by solving the linear system (15).

3.2 Discontinuous boundary data

When the capture circle $\mathcal{C}_r$ intersects the circle C_{m+1} for any $m = 0, 1, \ldots, \ell - 1$, then the boundary data in the BVP (2) will be discontinuous. Since the center of the capture

circle is the basepoint which is assumed to be $z_0 = 0$, the two intersection points of the two circles are

$$e^{\mathrm{i}\arg(z_{m+1})}\,(x \pm \mathrm{i}y),\qquad(18)$$

where

$$x = \frac{r^2 + |z_{m+1}|^2 - R_{m+1}^2}{2|z_{m+1}|},\quad y = \sqrt{r^2 - x^2}.\qquad(19)$$

There are several possible different domain regimes Ω_r as the radius r of the capture circle $\mathcal{C}_r$ increases. The domain Ω_r could be simply connected or multiply connected. For all possible cases, we need the following function $U_r(z)$ which will be needed to solve the BVP (2) when the boundary data is not continuous.

3.2.1 The function U_r

For $m = 0, 1, \ldots, \ell - 1$, assume that $r \in (|z_{m+1}| - R_{m+1}, |z_{m+1}| + R_{m+1})$ and the capture circle $\mathcal{C}_r$ intersects the circle C_{m+1} at the two points ξ_1 and ξ_2 given by (18). Let $\mathcal{C}_r'$ be the arc of $\mathcal{C}_r$ that lies outside C_{m+1} (colored blue in Figure 3(a,c)) and let C_{m+1}' be the arc of the circle C_{m+1} that lies inside $\mathcal{C}_r$ (colored red in Figure 3(a,c)). It then follows that

$$\hat{\mathcal{C}}_r = \mathcal{C}_r' \cup C_{m+1}' \cup \{\xi_1, \xi_2\}$$

is a piecewise smooth Jordan curve, see Figure 3(a,c). We assume that $\hat{\mathcal{C}}_r$ is oriented counterclockwise. Let $\hat{\Omega}_r$ be the simply connected domain in the interior of $\hat{\mathcal{C}}_r$, and let $U_r(z)$ be the unique solution of the following Dirichlet BVP:

$$\nabla^2 U_r(z) = 0 \quad \text{if } z \in \hat{\Omega}_r;\qquad(20\text{a})$$
$$U_r(z) = 1 \quad \text{if } z \in C_{m+1}';\qquad(20\text{b})$$
$$U_r(z) = 0 \quad \text{if } z \in \mathcal{C}_r'.\qquad(20\text{c})$$

Note that the boundary data of the BVP (20) on $\hat{\mathcal{C}}_r$ is not continuous.

We can find the exact solution of the BVP (20). We first use the affine map

$$\Phi(z) = e^{-\mathrm{i}\arg(z_{m+1})}(z - z_0)$$

to translate and rotate the domain $\hat{\Omega}_r$ to obtain a domain $\tilde{\Omega}_r$ bounded by $\hat{L}_r = L_1 \cup L_2 \cup \{\zeta_1, \zeta_2\}$ where L_1 is the image of $\mathcal{C}_r'$, L_2 is the image of C_1', $\zeta_1 = \Phi(\xi_1)$, and $\zeta_2 = \Phi(\xi_2)$. Let ζ_3 be the bisection point of the arc joining ζ_1 to ζ_2 so that $\zeta_1, \zeta_3, \zeta_2$ are ordered counterclockwise. Note that $\zeta_2 = \overline{\zeta_1}$ and ζ_3 is on the positive real line. The Möbius transform

$$\Psi(z) = e^{-\mathrm{i}\alpha}\frac{z - \zeta_2}{z - \zeta_1},\quad \alpha = \arg\left(\frac{r - \zeta_2}{\zeta_1 - r}\right) = 2\tan^{-1}\left(\frac{r - x}{y}\right) = 2\tan^{-1}\left(\sqrt{\frac{r - x}{r + x}}\right),\quad(21)$$

transplants the domain $\tilde{\Omega}_r$ onto the wedge

$$\{z = re^{\mathrm{i}\theta} \mid r > 0,\ 0 < \theta < \nu\},\quad \nu = \beta - \alpha,\quad \beta = \arg\left(\frac{\zeta_3 - \zeta_2}{\zeta_3 - \zeta_1}\right) = 2\tan^{-1}\left(\frac{y}{x - \zeta_3}\right),$$

and hence, using trigonometric identities, we have

$$\nu = 2\tan^{-1}\left(\frac{y^2 - (r - x)(x - \zeta_3)}{y(r - \zeta_3)}\right)$$

which can be written as

$$\nu = 2\tan^{-1}\left(\frac{(r - x)(2r - d)}{yd}\right) = 2\tan^{-1}\left(\frac{2r - d}{d}\sqrt{\frac{r - x}{r + x}}\right),\quad d = r - \zeta_3.$$

Thus, the solution $U_r(z)$ of the BVP (20) is given for $z \in \hat{\Omega}_r$ by

$$U_r(z) = \frac{1}{\pi}\,\mathrm{Im}\log\left(\Psi(\Phi(z))\right)^{\pi/\nu} = \frac{1}{\nu}\arg\left(e^{-\mathrm{i}\alpha}\frac{\Phi(z) - \zeta_2}{\Phi(z) - \zeta_1}\right) = \frac{1}{\nu}\arg\left(e^{-\mathrm{i}\alpha}\frac{z - \xi_2}{z - \xi_1}\right).\quad(22)$$
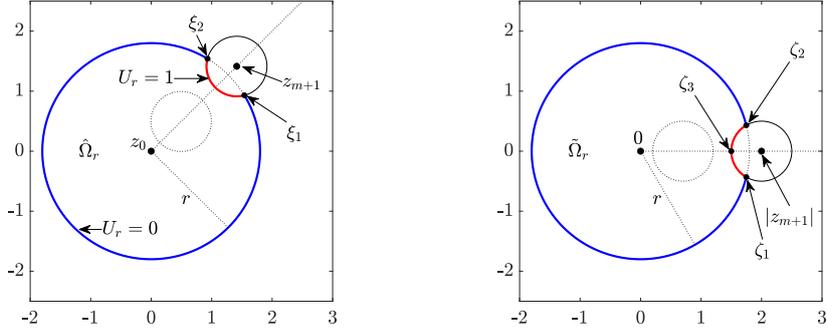
Figure 5: On the left, schematic of the domain $\hat{\Omega}_r$ (for $m = 1$) and the boundary values of the function U_r on the two arcs $\mathcal{C}_2'$ (red) and $\mathcal{C}_r'$ (blue). On the right, the corresponding domain $\tilde{\Omega}_r$.

3.2.2 Ω_r is simply connected

When $m = 0$ and $r \in (|z_1| - R_1, |z_1| + R_1)$, the capture circle $\mathcal{C}_r$ intersects the circle C_1 at the two points ξ_1 and ξ_2 given by (18). Note that all the other circles $C_2, \ldots, C_\ell$ are outside $\mathcal{C}_r$. In this case, the domain Ω_r is the same as the domain $\hat{\Omega}_r$ in Section 3.2.1 and hence both BVPs (2) and (20) are identical. Thus the solution $u(z)$ to the BVP (2) is the same as the solution $U_r(z)$ to the BVP (20) given by (22). Since $\Phi(z_0) = 0$ and $\zeta_1 = \overline{\zeta_2}$, we have

$$g(r) = u(z_0) = U_r(z_0) = \frac{1}{\nu} \arg\left(e^{-i\alpha} \frac{\zeta_2}{\overline{\zeta_2}}\right) = \frac{2 \arg(\zeta_2) - \alpha}{\nu}. \tag{23}$$

It can be noted that $\arg(\zeta_2) = \tan^{-1}(y/x)$ where x and y are given in (19), and hence, by (21) and using trigonometric identities, we obtain

$$2 \arg(\zeta_2) - \alpha = 2 \tan^{-1}(y/x) - 2 \tan^{-1}\left(\frac{r - x}{y}\right) = 2 \tan^{-1}\left(\frac{r - x}{y}\right) = 2 \tan^{-1}\left(\sqrt{\frac{r - x}{r + x}}\right).$$

Thus, we have

$$g(r) = \frac{\tan^{-1}\left(\sqrt{\frac{r-x}{r+x}}\right)}{\tan^{-1}\left(\frac{2r-d}{d}\sqrt{\frac{r-x}{r+x}}\right)}. \tag{24}$$

This is equivalent to the formula given in [16, Eq. (21.6)].

3.2.3 Ω_r is multiply connected

For $1 \le m \le \ell - 1$ and $r \in (|z_{m+1}| - R_{m+1}, |z_{m+1}| + R_{m+1})$, the capture circle $\mathcal{C}_r$ intersects the circle C_{m+1} at the two points ξ_1 and ξ_2 given by (18). Note that the circles $C_1, \ldots, C_m$ are inside $\mathcal{C}_r$ and the circles $C_{m+2}, \ldots, C_\ell$ are outside $\mathcal{C}_r$.

In this case, the domain Ω_r is a multiply connected domain of connectivity $m + 1$ and

$$\partial \Omega_r = C_1 \cup \cdots \cup C_m \cup \hat{\mathcal{C}}_r.$$

The solution $u(z)$ to the BVP (2) can be written as

$$u(z) = U_r(z) + v(z) \tag{25}$$

where $U_r(z)$ is given by (22) and $v(z)$ is a solution to the BVP

$$\nabla^2 v(z) = 0 \qquad\qquad \text{if } z \in \Omega_r; \tag{26a}$$
$$v(z) = 1 - U_r(z) \qquad\qquad \text{if } z \in C_1 \cup \cdots \cup C_m; \tag{26b}$$
$$v(z) = 0 \qquad\qquad \text{if } z \in \hat{\mathcal{C}}_r. \tag{26c}$$

Note that the boundary conditions of the BVP (26) are now continuous and hence solving the BVP (26) is much easier than solving the original problem (2). Also note that the external boundary $\hat{\mathcal{C}}_r$ of the domain Ω_r is not a circle as in the continuous data case discussed in Section 3.1.

However, the domain Ω_r is still of the type of domain G considered in Section 2 with $\Gamma_0 = \hat{\mathcal{C}}_r$ and $\Gamma_k = C_k$ for $k = 1, \ldots, m$. It then follows from (11) that

$$v(z_0) = c - \sum_{j=1}^{m} a_j \log |z_0 - \alpha_j|$$

where the $m + 1$ unknown real constants $c, a_1, \ldots, a_m$ are obtained by solving the linear system (15), and where $\gamma(\zeta) = 0$ for $\zeta \in \Gamma_0$ and $\gamma(\zeta) = 1 - U_r(\zeta)$ for $\zeta \in \Gamma_j$ for $j = 1, 2, \ldots, m$. Finally, it follows from (1) and (25) that

$$g(r) = u(z_0) = U_r(z_0) + v(z_0).$$

3.3 Numerical examples

We assume that Ω is the unbounded multiply connected domain in the exterior of ℓ disks with centers z_k and radii $R_k = 0.4$, $k = 1, 2, \ldots, \ell$. We assume that the basepoint is $z_0 = 0$. For the centers, we consider three cases:

(I) $z_k = k$, $k = 1, 2, \ldots, \ell$.

(II) $z_k = k\, e^{\theta_k \mathrm{i}}$, where $\theta_k = 2(k-1)\pi/\ell$, $k = 1, 2, \ldots, \ell$.

(III) $z_k = k\, e^{\tau_k \mathrm{i}}$, $k = 1, 2, \ldots, \ell$, where, for each $k = 1, 2, \ldots, \ell$, τ_k is a random number in $(0, 2\pi)$.

The values of the g-function $g(r)$ for the three cases are shown in Figure 7 for $\ell = 5$ (left) and $\ell = 10$ (right).
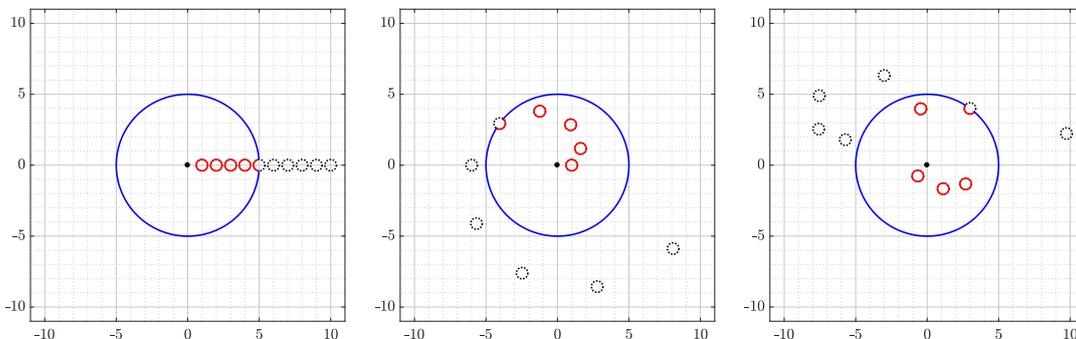
Figure 6: The domain Ω_r for the three unbounded multiply connected circular domain cases for $\ell = 10$.

4 Domains bounded by slits

Let Ω be an unbounded multiply connected domain in the exterior of ℓ non-overlapping rectilinear slits $I_j = [a_j, b_j]$ where a_j and b_j are real numbers. We assume that these slits are arranged such that

$$0 < a_1 < b_1 < a_2 < b_2 < \cdots < a_\ell < b_\ell.$$

For a given $r > 0$, the capture circle $\mathcal{C}_r$ intersects at most one of the slits $I_1, I_2, \ldots, I_\ell$ (see Figure 4 for an example when $\ell = 2$).

As in the previous section, we also have here two classes of boundary data to be considered as in the following subsections.
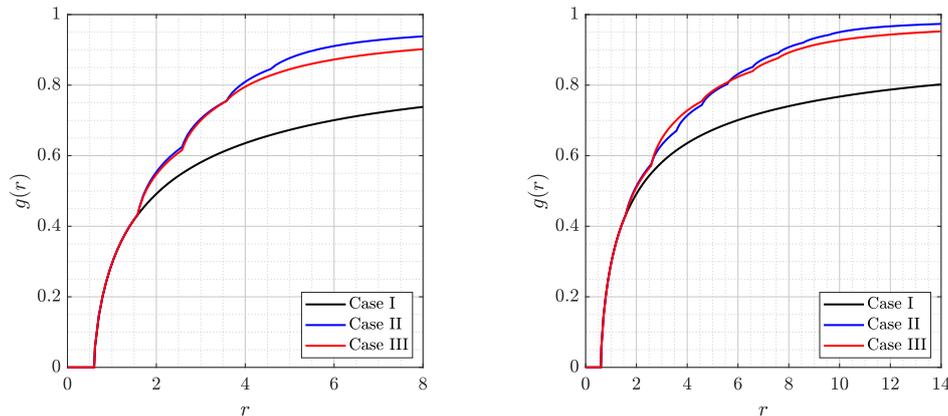
Figure 7: The values of the g-function $g(r)$ for $\ell = 5$ (left) and $\ell = 10$ (right).

4.1 Continuous boundary data

Suppose that the capture circle $\mathcal{C}_r$ does not intersect any of the slits $I_1, \ldots, I_\ell$. For $m = 0, 1, 2, \ldots, \ell$, we assume that the slits $I_1, \ldots, I_m$ are inside $\mathcal{C}_r$ and the slits $I_{m+1}, \ldots, I_\ell$ are outside $\mathcal{C}_r$. That is, all slits $I_1, \ldots, I_\ell$ are outside the capture circle $\mathcal{C}_r$ for $m = 0$ and all slits $I_1, \ldots, I_\ell$ are inside the capture circle $\mathcal{C}_r$ for $m = \ell$. See Figure 4(b,d) for $m = 1$ and 2, respectively.

For all values of r such that all slits $I_1, \ldots, I_\ell$ are outside the capture circle $\mathcal{C}_r$ (i.e. $m = 0$), we have $g(r) = 0$. If $m \geq 1$, the domain Ω_r is a bounded multiply connected domain of connectivity $m + 1$ and

$$\partial \Omega_r = I_1 \cup \cdots \cup I_m \cup \mathcal{C}_r.$$

Note that, in the BVP (2), we have $E_r = I_1 \cup \cdots \cup I_m$ and hence $\partial \Omega_r \backslash E_r = \mathcal{C}_r$. That is, the function $u(z)$ is the harmonic measure of $I_1 \cup \cdots \cup I_m$ with respect to the domain Ω_r.

The domain Ω_r here is not bounded by Jordan curves and hence the BIE method presented in Section 2 is not directly applicable to such a domain. This obstacle will be overcome using conformal mappings. Consider the unbounded multiply connected domain $\hat{\Omega}$ lying in the exterior of the m slits $I_1, \cdots, I_m$. We can use the iterative method presented in [23] to find a conformally equivalent unbounded multiply connected domain $\hat{G}$ lying in the exterior of m circles $\Gamma_1, \cdots, \Gamma_m$ and a conformal mapping $w = \phi(z)$ from $\hat{G}$ onto $\hat{\Omega}$. We omit the details of the iterative method here and refer the reader to [23] (see also [8]). Note that the circle $\mathcal{C}_r$, which is the outer boundary of Ω_r, is within the domain $\hat{\Omega}$. Using the inverse mapping $z = \phi^{-1}(w)$, the circle $\mathcal{C}_r$ will be mapped onto a smooth Jordan curve Γ_0 surrounding the m circles $\Gamma_1, \cdots, \Gamma_m$. Now, let G be the bounded multiply connected domain in the interior of Γ_0 and in the exterior of $\Gamma_1, \cdots, \Gamma_m$. Then G is conformally equivalent to Ω_r and $w = \phi(z)$ is a conformal mapping from G onto Ω_r. Since the Dirichlet BVP is invariant under conformal mapping, then the unique solution $u(z)$ of the BVP (2) is given by $u(z) = U(\phi^{-1}(z))$ where $U(z)$ is the unique solution of the following Dirichlet BVP:

$$\nabla^2 U(z) = 0, \qquad z \in G; \tag{27a}$$

$$U(z) = \hat{\gamma}(z), \qquad z \in \Gamma = \partial G; \tag{27b}$$

where

$$\hat{\gamma}(z) = \begin{cases} 0, & z \in \Gamma_0, \\ 1, & z \in \Gamma_j, \quad j = 1, \ldots, m. \end{cases} \tag{28}$$

Then,

$$g(r) = u(z_0) = U(\phi^{-1}(z_0)),$$

where $U(\phi^{-1}(z_0))$ can be computed using the BIE method presented in Section 2.

4.2 Discontinuous boundary data

When the capture circle $\mathcal{C}_r$ intersects the slit I_{m+1} for any $m = 0, 1, \ldots, \ell - 1$, then the boundary data in the BVP (2) will be discontinuous. Since the center of the capture circle is the basepoint which is assumed to be $z_0 = 0$, the single intersection point is $c_{m+1} = r$.

As before, there are several possible different domain regimes Ω_r as the radius r of the capture circle $\mathcal{C}_r$ increases. The domain Ω_r can be simply or multiply connected. In all cases, we need the following function $V_r(z)$ which will be used to solve the BVP (2) when the boundary data is not continuous.

4.2.1 The function V_r

For $m = 0, 1, \ldots, \ell-1$, assume that $r \in (a_{m+1}, b_{m+1})$ so that the capture circle $\mathcal{C}_r$ intersects the slit I_{m+1} at the point $c_{m+1} = r$. Let I'_k be the portion of the slit I_k that lies inside $\mathcal{C}_r$ (colored red in Figure 4(a,c)). Let $\hat{\Omega}_r$ be the bounded simply connected domain such that

$$\partial \hat{\Omega}_r = \mathcal{C}_r \cup I'_k,$$

and let $V_r(z)$ be the unique solution of the following Dirichlet BVP in $\hat{\Omega}_r$:

$$\nabla^2 V_r(z) = 0 \quad \text{if } z \in \hat{\Omega}_r, \tag{29a}$$

$$V_r(z) = \gamma(z) \quad \text{if } z \in \partial \hat{\Omega}_r, \tag{29b}$$

where

$$\gamma(z) = \begin{cases} 1, & z \in I'_k, \\ 0, & z \in \mathcal{C}_r. \end{cases} \tag{30}$$

The exact solution of the BVP (29) can be found. To this end, consider the conformal mapping

$$w = \psi(z) = \mathrm{i}\sqrt{\left(\frac{r-z}{r+z}\right)^2 - \left(\frac{r-a_k}{r+a_k}\right)^2} \tag{31}$$

which transplants $\hat{\Omega}_r$ onto the upper half-plane such that I'_k is mapped onto the finite slit $[-w_k, w_k]$ on the real line and $\mathcal{C}_r$ is mapped onto $(\mathbb{R} \cup \{\infty\}) \backslash [-w_k, w_k]$, where

$$w_k = \frac{r - a_k}{r + a_k} \in (0, 1). \tag{32}$$

The branch of the square root in (31) is chosen such that $\mathrm{Re}\,\sqrt{z} \geq 0$ for $z \in \mathbb{C}$. Thus, the solution $V_r(z)$ of the BVP (29) is given for $z \in \hat{\Omega}_r$ by

$$V_r(z) = \frac{1}{\pi} \arg\left(\frac{\psi(z) - w_k}{\psi(z) + w_k}\right). \tag{33}$$

4.2.2 Ω_r is simply connected

When $m = 0$ and $r \in (a_1, b_1)$, the capture circle $\mathcal{C}_r$ intersects the slit I_1 at the point $c_1 = r$, and all the other slits $I_2, \ldots, I_\ell$ are outside $\mathcal{C}_r$. In this case, the domain Ω_r is the same as the domain $\hat{\Omega}_r$ in Section 4.2.1 and hence the BVPs (2) and (29) are identical. Thus the solution $u(z)$ to the BVP (2) is the same as the solution $V_r(z)$ to the BVP (29) given by (33).

It follows from (31) that

$$\psi(z_0) = \psi(0) = \mathrm{i}\sqrt{1 - w_k^2}$$

and hence (33) implies

$$V_r(z_0) = \frac{1}{\pi} \arg\left(\frac{\mathrm{i}\sqrt{1-w_k^2} - w_k}{\mathrm{i}\sqrt{1-w_k^2} + w_k}\right) = \frac{2}{\pi} \arg\left(\sqrt{1-w_k^2} + \mathrm{i}w_k\right).$$

Finally, we have

$$g(r) = V_r(z_0) = \frac{2}{\pi} \tan^{-1}\left(\frac{w_k}{\sqrt{1-w_k^2}}\right) = \frac{2}{\pi} \tan^{-1}\left(\frac{r - a_k}{2\sqrt{ra_k}}\right). \tag{34}$$

4.2.3 Ω_r is multiply connected

For $1 \le m \le \ell - 1$ and $r \in (a_{m+1}, b_{m+1})$, the capture circle $\mathcal{C}_r$ intersects the slit I_{m+1} at the point $c_{m+1} = r$. Note that the slits $I_1, \ldots, I_m$ are inside $\mathcal{C}_r$ and the slits $I_{m+2}, \ldots, I_\ell$ are outside $\mathcal{C}_r$. In this case, the domain Ω_r is a bounded multiply connected domain of connectivity $m + 1$ and

$$\partial\Omega_r = I_1 \cup \cdots \cup I_m \cup I'_{m+1} \cup \mathcal{C}_r,$$

where $I'_{m+1} \cup \mathcal{C}_r$ is the outer boundary of Ω_r. We can write the solution $u(z)$ to the BVP (2) as

$$u(z) = V_r(z) + v(z)$$

where $V_r(z)$ is given by (33) and $v(z)$ is a solution to the following Dirichlet BVP:

$$\nabla^2 v(z) = 0 \quad \text{if } z \in \Omega_r; \tag{35a}$$
$$v(z) = \hat{\gamma}(z) \quad \text{if } z \in \partial\Omega_r, \tag{35b}$$

where

$$\hat{\gamma}(z) = \begin{cases} 1 - V_r(z), & z \in I_1 \cup \cdots \cup I_m, \\ 0, & z \in I'_{m+1} \cup \mathcal{C}_r. \end{cases} \tag{36}$$

We point out that the boundary data of the BVP (26) is now continuous. However, the boundary components of the domain Ω_r are not Jordan curves and hence this problem can not be solved using the above described BIE method as in Section 3.2.3 when Ω was a circular domain. Thus, in the current case, we will first use conformal mappings to map Ω_r onto a domain G bounded by smooth Jordan curves where we can then use our BIE method.

The mapping function $w = \psi(z)$ given by (31) maps the external boundary $I'_{m+1} \cup \mathcal{C}_r$ of Ω_r onto $\tilde{I}_0 = \mathbb{R} \cup \{\infty\}$ and maps the slits $I_1, \cdots, I_m$ onto slits $\tilde{I}_1, \ldots, \tilde{I}_m$, respectively, on the positive imaginary axis. Thus, $w = \psi(z)$ conformally maps the bounded multiply connected domain Ω_r onto the unbounded multiply connected domain $\tilde{\Omega}_r$ consists of the upper half-plane with m rectilinear slits. For the domain $\tilde{\Omega}_r$, we use the iterative method presented in [23] to find a multiply connected circular domain G in the interior of the unit circle Γ_0 and in the exterior of m circles $\Gamma_1, \ldots, \Gamma_m$ and a conformal mapping $w = \Phi(\zeta)$ from the domain G onto the domain $\tilde{\Omega}_r$ such that $\Phi(\Gamma_j) = \tilde{I}_j$, $j = 0, 1, \ldots, m$. We can compute the circular domain G such that $0 \in G$, and

$$\Phi(\mathrm{i}) = \infty, \quad \Phi(0) = \psi(z_0) = \mathrm{i}\sqrt{1-w_k^2}$$

where w_k is given by (32). Hence, the mapping function

$$z = \psi^{-1}(\Phi(\zeta))$$

conformally maps the domain G onto the domain Ω_r such that the inner curves $\Gamma_1, \dots, \Gamma_m$ are mapped onto the slits $I_1, \dots, I_m$, and the outer boundary Γ_0 is mapped onto the outer boundary $I'_{m+1} \cup \mathcal{C}_r$ of Ω_r. Consequently, the solution $v(z)$ to the BVP (35) is given by

$$v(z) = V(\Phi^{-1}(\psi(z))), \quad z \in \Omega_r, \tag{37}$$

where $V(\zeta)$ is the unique solution to the following Dirichlet BVP in the domain G:

$$\nabla^2 V(\zeta) = 0 \quad \text{if } \zeta \in G; \tag{38a}$$
$$V(\zeta) = \tilde{\gamma}(\zeta) \quad \text{if } \zeta \in \Gamma = \partial G, \tag{38b}$$

where

$$\hat{\gamma}(\zeta) = \begin{cases} 1 - V_r(\psi^{-1}(\Phi(\zeta))), & \zeta \in \Gamma_1 \cup \dots \cup \Gamma_m, \\ 0, & \zeta \in \Gamma_0. \end{cases} \tag{39}$$

The BVP (38) can then be solved easily using the BIE method as described in Section 2. By computing the solution $V(\zeta)$ to the BVP (38), we obtain the solution $v(z)$ to the BVP (35) by (37). Hence,

$$g(r) = u(z_0) = V_r(z_0) + v(z_0) = V_r(z_0) + V(\Phi^{-1}(\psi(z_0))) = V_r(z_0) + V(0).$$

4.3 Numerical examples

Example 1 We assume that the basepoint is $z_0 = 0$ and Ω_k is the unbounded multiply connected domain in the exterior of the closed set E_k for $k = 0, 1, 2, 3, 4$ where $E_0 = [1, 8]$, $E_1 = [1, 2]$, $E_2 = [1, 2] \cup [3, 4]$, $E_3 = [1, 2] \cup [3, 4] \cup [5, 6]$, and $E_4 = [1, 2] \cup [3, 4] \cup [5, 6] \cup [7, 8]$. The values of the g-function $g(r)$, for $k = 0, 1, 2, 3, 4$, computed with $n = 2^{13}$ are shown in Figure 8.
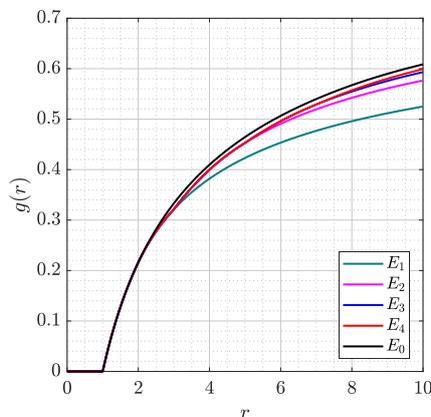
Figure 8: The values of the g-function $g(r)$ for Ω_k in Example 1 for $k = 0, 1, 2, 3, 4$.

Example 2 Let the sets E_k be defined recursively by

$$E_k = \frac{1}{3}(E_{k-1} + 2) \bigcup \frac{1}{3}(E_{k-1} + 4), \quad k \geq 1,$$

with $E_0 = [1, 2]$. Note that

$$\bigcap_{j=0}^{\infty} E_j$$

is the middle-thirds Cantor set of the interval $[1, 2]$. We assume that the basepoint is $z_0 = 0$ and Ω_k is the unbounded multiply connected domain in the exterior of the closed set E_k.

The graphs of the g-function $g(r)$, for $k = 0, 2, 4, 8, 16, 32$, computed with $n = 2^{13}$ are shown in Figure 9. These graphs illustrate that the g-function for the domain Ω_k is non-constant and exhibits a finite number of points where its first derivative is discontinuous. Note that, for this domain Ω_k, the graphs of the h-function for $k = 16$ and $k = 32$ are presented in [8, Fig 8]. In contrast, these graphs consist of a finite number of horizontal line segments which correspond to those values of r when the capture circle is not intersecting the slits and is otherwise an increasing function.

As is apparent in Figure 9, the values of the g-function, as a function of k, decrease slightly as k increases. However, it seems that these graphs approach some curve as k increases and it is difficult to tell the graphs apart from each other, e.g., it is not possible in Figure 9 to distinguish between the graphs for $k = 16$ and $k = 32$.
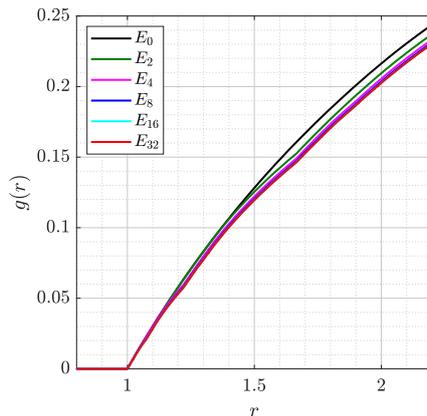
Figure 9: The values of the g-function $g(r)$ for Ω_k in Example 2 for $k = 0, 2, 4, 8, 16, 32$.

5 Other domains

In the previous two sections, we assumed that the capture circle intersects at most one of the boundary components. The presented method can be extended to the cases when the capture circle intersects more than one boundary component. By way of example, consider the unbounded multiply connected domain Ω in the exterior of m disks having centers and radii

$$z_k = 5\, e^{2\pi(k-1)\mathrm{i}/\ell}, \quad R_k = 1, \quad k = 1, 2, \ldots, \ell. \tag{40}$$

We assume that the basepoint is $z_0 = 0$. It is clear that $g(r) = 0$ for $r \in [0, 4]$. For $r \in (4, 6)$, the domain Ω_r is a simply connected polycircular arc domain as shown in Figure 10 (left) for $\ell = 10$. Then

$$g(r) = u(z_0)$$

where $u(z)$ is the unique solution to the BVP (2) where E_r is the union of the parts of the circles $C_1, \ldots, C_\ell$ that lie inside the capture circle $\mathcal{C}_r$ (shown in red in Figure 10 (left)). In this case, the capture circle intersects all the circles $C_1, \ldots, C_\ell$. The intersection points are denoted by ξ_{2j-1} and ξ_{2j}, $j = 1, 2, \ldots, \ell$. We assume $\partial\Omega_r$ is oriented counterclockwise and that the points $\xi_1, \ldots, \xi_{2\ell}$ are ordered counterclockwise on the capture circle $\mathcal{C}_r$.

When $r \in (4, 6)$, we let $\zeta = \psi(z)$ be the conformal mapping from the simply connected polycircular arc domain Ω_r onto the unit disk $\mathbb{D}$ such that $\psi(0) = 0$. Then $\zeta = \psi(z)$ maps the boundary $\partial\Omega_r$ onto the unit circle L such that the points $\zeta_j = \psi(\xi_j)$, $j = 1, \ldots, 2\ell$, are on the unit circle and oriented counterclockwise. For $k = 1, 2, \ldots, \ell$, let L_k be the arc on the unit circle that connects ζ_{2k-1} to ζ_{2k} (in the counterclockwise direction). Let also $\hat{L}_k$ be the arc on the unit circle that connects ζ_{2k} to ζ_{2k+1} (in the counterclockwise direction), where $\zeta_{2\ell+1} = \zeta_1$. The mapping function $\zeta = \psi(z)$ can be computed as described in [24].

Let $w = \phi(\zeta)$ be the Möbius transformation from the unit disk $\mathbb{D}$ onto the upper half-plane such that $\phi(\zeta_1) = \infty$ and $\phi(\zeta_{\ell+1}) = 0$. Hence,

$$w = \phi(\zeta) = \frac{\zeta^* - \zeta_1}{\zeta^* - \zeta_{\ell+1}} \frac{\zeta - \zeta_{\ell+1}}{\zeta - \zeta_1}$$

where $\zeta^* = \zeta_{\lfloor (3\ell/2)+1 \rfloor}$ and $\lfloor \cdot \rfloor$ denotes the floor function. The point ζ^* is chosen such that it will be mapped onto 1 on the positive real line so that the arc connecting ζ_1 and $\zeta_{\ell+1}$ (in the counterclockwise direction) is mapped onto the negative real line. Then, for $j = 2, \ldots, 2\ell$, the points $x_j = \phi(\zeta_j)$ will be on the real line such that $x_j < x_{j+1}$. Let I_j and $\hat{I}_j$ be the images of the arcs L_j and $\hat{L}_j$ under the Möbius transformation $w = \phi(\zeta)$, respectively. Then $I_2, \ldots, I_\ell, \hat{I}_1, \ldots \hat{I}_{\ell-1}$ are finite intervals and $I_1, \hat{I}_\ell$ are infinite intervals on the real line.

Now, the function

$$U(w) = \sum_{j=2}^{2\ell} \frac{(-1)^j}{\pi} \arg(w - x_j)$$

is harmonic on the upper half-plane with

$$U(w) = \begin{cases} 1, & \zeta \in I_1 \cup \cdots \cup I_\ell, \\ 0, & \zeta \in \hat{I}_1 \cup \cdots \cup \hat{I}_\ell. \end{cases}$$

The branch of $\arg(\cdot)$ is chosen such that $\arg(-1) = \pi$. Then the unique solution $u(z)$ to the BVP (2) is given by

$$u(z) = U(\phi(\psi(z))) = \sum_{j=2}^{2\ell} \frac{(-1)^j}{\pi} \arg\left(\phi(\psi(z)) - \phi(\psi(\xi_j))\right),$$

and hence the g-function $g(r)$ can be computed via

$$g(r) = u(z_0) = u(0).$$

Finally, when $r > 6$, the domain Ω_r is a bounded multiply connected circular domain of connectivity $\ell + 1$. The domain Ω_r in this case is of the type considered in Section 2 with $G = \Omega_r$, $m = \ell$, and the function γ as in (16). Hence, $g(r) = u(z_0)$ where $u(z_0)$ can be computed as in (11).

The graphs of the g-function $g(r)$ for several values of ℓ are shown in Figure 10. In this example, the boundary components of the domain Ω surrounding the basepoint $z_0 = 0$ which, as expected, results in $g(r) \to 1$ more rapidly when there are more boundary components compared to when there are fewer.

6 Bounded domains

To complete our study of the g-function in this paper, it is worth demonstrating that the presented method can be used in a straightforward manner for bounded domains Ω. This is briefly described in this section through an example for the domains Ω in Figure 6 but make them bounded domains with adding an outer boundary component which is the circle with center $z_0 = 0$ and radius $R_0 = 12$. For $0 \le r < 12$, the domain Ω_r here is the same as in the unbounded domain case in Figure 6. Hence, the values of $g(r)$ for $0 \le r < 12$ are the same as the values for the unbounded case as presented in Figure 7. For all values of r such that $r \ge 12$, we will have $\Omega_r = \Omega$ and hence $g(r) = 1$. The graphs of the g-function $g(r)$ for the three cases with $\ell = 10$ are shown in Figure 11. All graphs exhibit a fixed jump when $r = 12$.
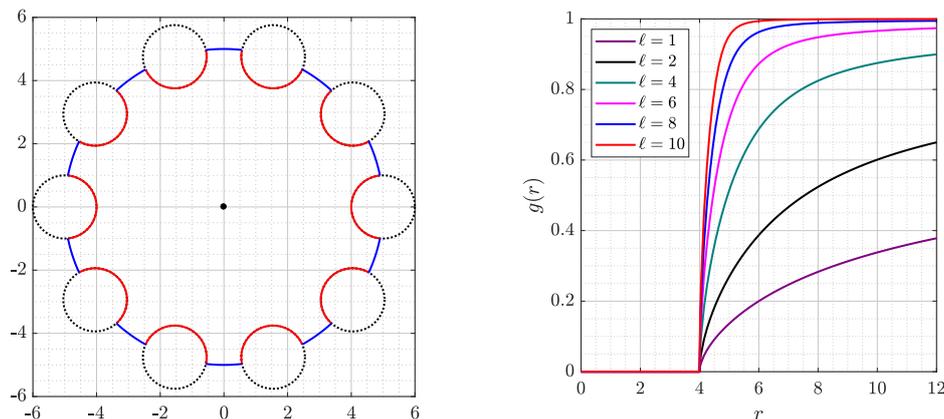
Figure 10: The domain Ω_r for the centers and radii given in (40) for $\ell = 10$ and $r = 5$ (left) and the values of the g-function $g(r)$ for several values of ℓ (right).
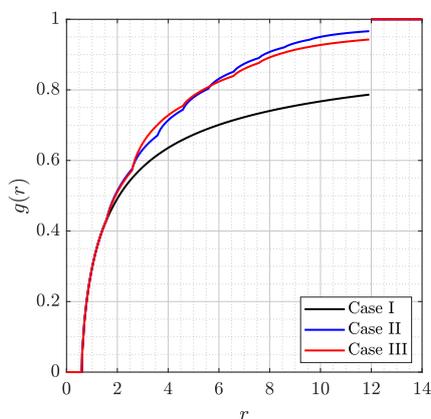
Figure 11: The values of the g-function $g(r)$ for the three cases in Figure 6 made bounded domains by adding an outer boundary component $|z| = 12$.

7 Conclusion

This paper has shown how to make numerical computations of the g-function associated with various multiply connected planar domains bounded by either rectilinear slits or circles. These g-functions are connected to their h-function counterparts, and both can be interpreted in terms of the motion of a Brownian particle released from some basepoint in the domain over which they are defined. We used a combination of conformal mapping techniques and a well-established boundary integral equation method to perform our calculations, and several graphs of g-functions have been plotted.

This work is the first attempt at computing the g-function in multiply connected domains. The graphs of the g-functions presented in this paper provide some insight into the properties of these g-functions and how they compare to the graphs of their h-function counterparts shown in [7, 8, 9]. However, much numerical work still remains to be done; in particular, to compute g-functions associated with domains bounded by curves other than circles and rectilinear slits, and for different basepoint locations.

References

[1] G.D. Anderson, M.K. Vamanamurthy & M. Vuorinen, Conformal Invariants. Inequalities and Quasiconformal Maps, Wiley-Interscience, New York, 1997.

[2] A. Barton & L.A. Ward, A new class of harmonic measure distribution functions, *J. Geom. Anal.* 24 (4) (2014) 2035–2071.

[3] D.A. Brannan & W.K. Hayman, Research problems in complex analysis, *Bull. London Math. Soc.* 21 (1989) 1–35.

[4] D.G. Crowdy, Solving Problems in Multiply Connected Domains, SIAM, Philadelphia, 2020.

[5] D.G. Crowdy & J.S. Marshall, Green's functions for Laplace's equation in multiply connected domains, *IMA J. Appl. Math.* 72 (2007) 278–301.

[6] J.B. Garnett & D.E. Marshall, Harmonic Measure, Cambridge University Press, Cambridge, 2008.

[7] C.C. Green, A. Mahenthiram & L.A. Ward, Harmonic-measure distribution functions of multiply connected domains with various geometries, *Proc. R. Soc. A*, submitted.

[8] C.C. Green & M.M.S. Nasser, Towards computing the harmonic-measure distribution function for the middle-thirds Cantor set, *J. Comput. Appl. Math.* 448 (2024), 115903.

[9] C.C. Green, M.A. Snipes, L.A. Ward & D.G. Crowdy, Harmonic-measure distribution functions for a class of multiply connected symmetrical slit domains, *Proc. R. Soc. A* 478 (2259) (2022) 20210832.

[10] L. Greengard and Z. Gimbutas, FMMLIB2D: A MATLAB toolbox for fast multipole method in two dimensions, version 1.2. 2019, `https://github.com/zgimbutas/fmmlib2d`. Accessed 1 Feb 2024.

[11] P. Henrici, Applied and Computational Complex Analysis, Vol. 3, John Wiley & Sons, New York, 1986.

[12] S. Kakutani, Two-dimensional Brownian motion and harmonic functions, *Proc. Imp. Acad. Tokyo* 20 (1944) 706–714.

[13] S. Kakutani, Two-dimensional Brownian motion and the type problem of Riemann surfaces, *Proc. Japan Acad.* 21 (1945) 138–140.

[14] I. Karatzas, S. Shreve, Brownian Motion and Stochastic Calculus, 2$^{\text{nd}}$ ed., Springer Science & Business Media, 2012.

[15] A. Mahenthiram, Computing h-functions of some planar simply connected two-dimensional regions, *Taiwanese J. Math.* 27 (2023) 931–952.

[16] A. Mahenthiram, Harmonic-Measure Distribution Functions, and Related Functions, for Simply Connected and Multiply Connected Two-Dimensional Regions (PhD thesis), University of South Australia, 2024.

[17] A. Mahenthiram, Harmonic-measure distribution functions of simply connected and doubly connected polygonal domains, *J. Math. Anal. Appl.* 537 (2024) 128308.

[18] A. Mahenthiram, New harmonic-measure distribution functions of some simply connected planar regions in the complex plane, *Revista de la Unión Matemática Argentina*, Accepted.

[19] A. Mahenthiram, B.L. Walden & L.A. Ward, Stephenson's g-function for simply connected planar domains. In preparation.

[20] S.G. Mikhlin, Integral Equations and their Applications to Certain Problems in Mechanics, Mathematical Physics and Technology, Pergamon Press, Armstrong, 1957.

[21] M.M.S. Nasser, A.H.M. Murid & Z. Zamzamir, A boundary integral method for the Riemann–Hilbert problem in domains with corners, *Complex Var. Elliptic Equ.* 53 (2008) 989–1008.

[22] M.M.S. Nasser, Fast solution of boundary integral equations with the generalized Neumann kernel, *Electron. Trans. Numer. Anal.* 44 (2015) 189–229.

[23] M.M.S. Nasser & C.C. Green, A fast numerical method for ideal fluid flow in domains with multiple stirrers, *Nonlinearity* 31 (2018) 815–837.

[24] M.M.S. Nasser, O. Rainio, A. Rasila, M. Vuorinen, T. Wallace, H. Yu & X. Zhang, Polycircular domains, numerical conformal mappings, and moduli of quadrilaterals, *Adv. Comput. Math.* 48 (2022) 58.

[25] M.M.S. Nasser & M. Vuorinen, Numerical computation of the capacity of generalized condensers, *J. Comput. Appl. Math.* 377 (2020) 112865.

[26] M.A. Snipes & L.A. Ward, Harmonic measure distribution functions of planar domains: A survey, *J. Anal.* 24 (2016) 293–330.

[27] M. Tsuji, Potential Theory in Modern Function Theory, Chelsea Publ. Co., New York, 1975.

[28] B.L. Walden & L.A. Ward, Distributions of harmonic measure for planar domains, in: I. Laine, O. Martio (Eds.), Proceedings of 16th Nevanlinna Colloquium, Joensuu, Walter de Gruyter, Berlin, 1996, pp. 289–299.

[29] R. Wegmann & M.M.S. Nasser, The Riemann-Hilbert problem and the generalized Neumann kernel on multiply connected regions, *J. Comput. Appl. Math.* 214 (2008) 36–57.